energies

Article

Eddy–Viscosity Reynolds-Averaged Navier–Stokes Modeling of Air Distribution in a Sidewall Jet Supplied into a Room

Maria Hurnik, **Piotr Ciuman** and **Zbigniew Popiolek** *

Faculty of Energy and Environmental Engineering, Silesian University of Technology, Konarskiego 20, 44-100 Gliwice, Poland; maria.hurnik@polsl.pl (M.H.); piotr.ciuman@polsl.pl (P.C.)
* Correspondence: zbigniew.popiolek@polsl.pl; Tel.: +48-32-237-11-51

Abstract: Air velocity is one of the key parameters affecting the sensation of thermal comfort. In mixing ventilation, the air is most often supplied above the occupied zone, and the air movement in a room is caused by jets that generate recirculating flows. An effective tool for predicting airflow in a room is CFD numerical modeling. In order to reproduce the air velocity distribution, it is essential to select a proper turbulence model. In this paper, seven *Eddy–Viscosity RANS* turbulence models were used to carry out CFD simulations of a sidewall air jet supplied into a room through a wall diffuser. The goal was to determine which model was the most suitable to adopt in this type of airflow. The CFD results were validated using experimental data by comparing the gross and integral parameters, along with the parameters of the quasi-free jet model. The numerical results obtained for *Std k-ε* and *EVTM* models were most consistent with the measurements. Their error values slightly exceeded 15%. On the contrary, the *k-ω* and *RNG k-ε* models did not reproduce the quasi-free jet parameters correctly. The research findings can prove beneficial for simulating air distribution in supplied air jets during the initial conceptual phases of HVAC system design.

Keywords: ventilation; air distribution; sidewall jet; CFD prediction; validation; eddy viscosity turbulence model

Citation: Hurnik, M.; Ciuman, P.; Popiolek, Z. Eddy–Viscosity Reynolds-Averaged Navier–Stokes Modeling of Air Distribution in a Sidewall Jet Supplied into a Room. *Energies* **2024**, *17*, 1261. https://doi.org/10.3390/en17051261

Academic Editor: Annunziata D'Orazio

Received: 14 February 2024
Revised: 28 February 2024
Accepted: 1 March 2024
Published: 6 March 2024

1. Introduction

Properly organized air distribution in rooms should ensure thermal comfort and high air quality with the lowest possible energy consumption. Requirements regarding thermal conditions in rooms, depending on the category of the indoor environment, are specified in various standards [1,2]. The sensation of thermal comfort is significantly influenced by air velocity. This parameter can also improve the circulation and distribution of fresh air, which can reduce the concentration of pollutants and thus affect the air quality in the room, as well as limit the spread of viruses and bacteria. COVID-19 diffusion is a problem linked to indoor air ventilation [3,4]. Poor ventilation can lead to higher concentrations of viral particles, increasing the risk of infection among occupants. Effective indoor air ventilation plays a crucial role in mitigating the spread of COVID by diluting and removing airborne contaminants, thus reducing the likelihood of transmission within indoor environments.

In mixing ventilation, the air is most often supplied above the occupied zone, and the air movement in a room is caused by jets that generate recirculating, i.e., induced secondary flows. The air speed in the occupied zone is very highly correlated with the momentum flux of the supplied jet [5,6]. The terms velocity and speed are used as synonyms in everyday language. In this paper, we use these terms as defined in ANSI/ASHRAE 113-2005 [7]. According to this standard, velocity and speed are different physical quantities. Velocity is a vector quantity, $\vec{U} = i\,U_x + j\,U_y + k\,U_z$, while speed is a scalar quantity, i.e., it is the value of the modulus of the velocity vector, $W = \left|\vec{U}\right| = \left(U_x^2 + U_y^2 + U_z^2\right)^{1/2}$.

A comparison of various advanced air distribution systems, which mainly depend on the type and location of supplied jets, is presented in a prior review paper [8]. The simplest tool for designing air distribution systems is based on engineering models of ventilation air jets. However, these models do not provide complete information about the air distribution in the entire room. An effective tool for predicting airflow, both in the supplied jets and in the occupied zone, is CFD numerical modeling [5].

The quality of CFD modeling depends on many factors, such as the adopted turbulence model, the type of discretization grid and number of cells, the way the boundary conditions are defined, and others. All these factors are sources of uncertainty for the CFD calculation results. Therefore, validation of the CFD codes, which means assessing the uncertainty of simulation results by comparing them with experimental data, is necessary [9–12]. Uncertainty quantification analysis is essential for enhancing the reliability, robustness, and applicability of flow dynamic simulations in various engineering and scientific applications [13,14].

1.1. Turbulence Models

To obtain reliable CFD results, accurate turbulence modeling is necessary. The turbulence model should be selected and adapted to the type of flow. Some experience and knowledge in this field are also needed.

Air distribution in a room can be modeled with the use of various turbulence models that are available in computing software, e.g., Ansys CFX 22.1 [15]. The first group of turbulence models is the *Reynolds-Averaged Navier–Stokes Equation* (*RANS*), which includes turbulence models from *Eddy–Viscosity Models* (*EVM*) and *Reynolds Stress Models* (*RSM*) subgroups. Moreover, the *Unsteady RANS* (*URANS*) and vortex-resolving *Large Eddy Simulation* (*LES*) turbulence models are available. The *LES* technique directly solves the filtered Navier–Stokes equations, thus solving large scales of motion. Smaller scales are modeled with a suitable *sub-grid scale model* (*SGS*). A review and discussion of the prospects of *LES* development are presented in a previous paper [16].

The averaged equations of the *RANS* turbulence models include expressions containing the fluctuating components, the so-called Reynolds stresses, which are considered as the impact of turbulence on the average airflow. Their presence means that the system of the Reynolds equations is not a closed one. Each turbulence model based on time-averaging differs in the way it determines the values of Reynolds stress and, thus, creates the equations that close the system.

In the *EVM* group, the turbulent viscosity coefficient v_t is introduced to determine the values of Reynolds stress describing the local state of turbulence and, unlike the molecular coefficient v_m, it is a variable dependent on location and time. *EVM* models differ in the method of determining this coefficient. The names of the models are related to the number of transport equations based on which this coefficient is calculated. In the zero-equation model, the differential transport equations are not used to determine turbulent viscosity, and only algebraic equations containing empirical coefficients are used. However, the zero-equation model has a weak physical basis; it is not recommended for use in numerical predictions.

The one-equation *Eddy–Viscosity Transport Model* (*EVTM*) includes a single transport equation to determine the turbulent viscosity coefficient. One of the most popular turbulence models is the two-equation *k*-ε model, which consists of two differential transport equations: the turbulence kinetic energy *k* equation and the turbulence energy dissipation rate ε. Its modified form is the *Re-Normalisation Group* (*RNG*) *k*-ε model, in which the transport equations are the same, but the constants of the model are different. It was developed for highly turbulent isotropic flows. One of the advantages of another popular model, the two-equation *k*-ω model (in which *k* is the turbulence kinetic energy and ω is the turbulence vorticity), is that is provides a more accurate method of calculating the boundary-layer flows for low Reynolds numbers compared to the *k*-ε model. The model does not require the modifications that are necessary in this region in the *k*-ε model. It is used in the standard version, known as the *Wilcox k-ω* model, as well as in the *Baseline* (*BSL*) *k*-ω model and the *Shear Stress Transport* (*SST*) model created by combining it with the *k*-ε model. The *BSL* model integrates the *k*-ω model close to solid walls with the standard *k*-ε model presuming distance from them. The *SST* model is also a combination of the *k*-ω model (in the inner boundary layer) and the *k*-ε model (in the outer boundary layer and beyond), but additionally a limitation of the value of shear stress in the area of the reverse pressure gradient is implemented in it. This model is frequently recommended for calculating the airflow of supply jets. The *EVM RANS* turbulence models available in the ANSYS CFX 22.1 software are presented in Table 1.

Table 1. *EVM RANS* turbulence models available in the ANSYS CFX 22.1 software.

Zero Equation Model		
One-Equation Model	*EVTM* model	
Two-Equation Models	*k*-ε model	Standard *k*-ε
		RNG k-ε
	k-ω model	*Wilcox k*-ω
		BSL k-ω
		SST

In the one-equation *Eddy–Viscosity Transport Model* (*EVTM*) the transport equation of turbulent viscosity coefficient v_t is used:

$$\frac{\partial \rho}{\partial t}\overline{v}_t + \frac{\partial \rho V_j \overline{v}_t}{\partial x_j} = c_1 \rho \overline{v}_t S - c_2 \rho \left(\frac{\overline{v}_t}{L_{\nu k}}\right)^2 + \left[\left(\mu + \frac{\rho \overline{v}_t}{\sigma}\right)\frac{\partial \overline{v}}{\partial x_j}\right] \tag{1}$$

where $\overline{v}$ is the kinematic viscosity coefficient of the vortex, $\overline{v}_t$ is the turbulent viscosity coefficient of the vortex, and σ is a constant in the model. The model includes a decay term ${L_{\nu k}}^2$ which expresses the turbulence structure and is based on the Karman length scale.

The two-equation *k*-ε model consists of two differential transport equations:

- Turbulence kinetic energy k, which is a measure of the portion of energy flow that arises from velocity fluctuations:

$$\frac{\partial (\rho k)}{\partial t} + \frac{\partial}{\partial x_j}(\rho V_j k) = \frac{\partial}{\partial x_j}\left[\left(\mu + \frac{\mu_t}{\sigma_k}\right)\frac{\partial k}{\partial x_j}\right] + P_k - \rho\varepsilon + P_{kb} \tag{2}$$

- Turbulence energy dissipation rate ε, which is a measure of the conversion of turbulent kinetic energy into heat per unit time:

$$\frac{\partial (\rho \varepsilon)}{\partial t} + \frac{\partial}{\partial x_j}(\rho V_j \varepsilon) = \frac{\partial}{\partial x_j}\left[\left(\mu + \frac{\mu_t}{\sigma_\varepsilon}\right)\frac{\partial \varepsilon}{\partial x_j}\right] + \frac{\varepsilon}{k(C_{\varepsilon 1} P_k - C_{\varepsilon 2}\rho\varepsilon + C_{\varepsilon 1} P_{\varepsilon b})} \tag{3}$$

where $C_{\varepsilon 1}$, $C_{\varepsilon 2}$, σ_k and σ_ε are constants, P_{kb} and $P_{\varepsilon b}$ represent buoyant forces, and P_k expresses the production of turbulence caused by viscous forces:

$$P_k = \mu_t \left(\frac{\partial V_i}{\partial x_j} + \frac{\partial V_j}{\partial x_i}\right)\frac{\partial V_i}{\partial x_j} - \frac{2}{3}\frac{\partial V_k}{(\partial x_k)\left(3\mu_t \frac{\partial V_k}{\partial x_k} + \rho k\right)} \tag{4}$$

The turbulent viscosity coefficient is related to the model parameters through a correlation:

$$\nu_t = C_\mu \rho \frac{k^2}{\varepsilon} \tag{5}$$

where C_μ is a constant.

The *Re-Normalisation Group* (*RNG*) *k-ε* model is based on the mathematical technique of renormalisation group in reference to the Navier–Stokes equations. The transport equations for turbulence generation and its dissipation are the same as in the standard *k-ε* model, whereas the difference lies in the model's constants, the constant $C_{\varepsilon 1}$ is replaced by the constant $C_{\varepsilon 1RNG}$.

The standard *Wilcox k-ω* model assumes that the turbulent viscosity coefficient is related to the turbulence kinetic energy and the turbulence frequency through the equation:

$$\nu_t = \rho \frac{k}{\omega} \tag{6}$$

This model resolves two transport equations:

- Turbulence kinetic energy k:

$$\frac{\partial(\rho k)}{\partial t} + \frac{\partial}{\partial x_j}(\rho V_j k) = \frac{\partial}{\partial x_j}\left[\left(\mu + \frac{\mu_t}{\sigma_k}\right)\frac{\partial k}{\partial x_j}\right] + P_k - \beta' \rho k \omega + P_{kb} \tag{7}$$

- Turbulence vorticity ω:

$$\frac{\partial(\rho \omega)}{\partial t} + \frac{\partial}{\partial x_j}(\rho V_j \omega) = \frac{\partial}{\partial x_j}\left[\left(\mu + \frac{\mu_t}{\sigma_\omega}\right)\frac{\partial \omega}{\partial x_j}\right] + \alpha \frac{\omega}{k} P_k - \beta \rho \omega^2 + P_{\omega b} \tag{8}$$

where P_k is the turbulence generation rate, P_{kb} and $P_{\omega b}$ are terms accounting for thermal buoyancy. β', β, α, σ_k, σ_ω are constants in the model.

In the *Baseline* (*BSL*) *k*-ω model the Wilcox model equation is multiplied by an appropriately selected transition function F_1, while the transformed *k-ε* model is multiplied by the function 1-F_1. F_1 equals 1 near the surface and decreases to 0 outside the boundary layer (it is a function of distance from the wall). Therefore, at the edge of the boundary layer and outside it, the computational model becomes the standard *k-ε* model.

In the *SST* model, to reduce the shear stress values in separated flow, a limit is imposed on the calculated value of the turbulent viscosity coefficient:

$$\upsilon_t = \frac{\alpha_1 k}{\max(\alpha_1 \omega, SF_2)} \tag{9}$$

where F_2 is a blending function similar to F_1, which imposes a limitation only for the wall boundary layer. S is a quantity describing the rate of deformation.

1.2. Impact of Turbulence Model on CFD Results

The scientific literature includes examples of numerous research articles related to the numerical modeling of turbulent airflows in ventilated buildings. For many years, the influence of turbulence models from the *RANS*, *URANS*, and *LES* groups on the accuracy of predicting air distribution in rooms has been tested [17–24]. Various boundary conditions were also considered, i.e., inlet geometry, supply air velocity, Reynolds number, isothermal or non-isothermal flows, as well as inlet turbulence quantities: kinetic energy, intensity, dissipation rate, and scale length. Exemplary results from related studies are presented in refs [25–29]. Selected representative studies conducted in this area in the last few years are presented in Table 2.

Table 2. Overview of CFD validation studies of the air jets at different distribution systems in rooms.

Authors (Year) [Ref.]	Type of Airflow in Room	Method/Turbulence Model	Validation Method	Conclusion/Preferred Method and Turbulence Model
Gurgul and Fornalik-Wajs (2023) [30]	Impinging round jet	*SST k-ω*, *RNG k-ε*, *Intermittency Transition Model (SST k-ω)*, *Transition SST*, v^2-*f*	Comparison of calculated local Nusselt number distribution with literature experimental data and inlet velocity profile with *DNS* simulation	*SST k-ω*, *SST k-ω*, and *Intermittency Transition* models have the best agreement with experimental and numerical data
Chen et al. (2022) [31]	Forced, natural, and mixed convection	*RANS/Data-driven RNG k-ε*, *conventional RNG k-ε* *LES/WALE*, and *Smagorinsky–Lilly subgrid scale*	Artificial neural network was used to determine the coefficient of high-order terms; *RANS* validated with *LES*	Data-driven model is more accurate than conventional *RNG k-ε*
Hurnik et al. (2022) [32]	Sidewall jet, recirculating flow in an occupied zone	*URANS/Standard k-ε*, *wall-modeled LES/S-Omega subgrid-scale model*	Comparison of local, gross, and integral parameters in the jet zone, and cumulative distribution of mean air speed in the occupied zone with LDA [1] and LVTA [2]	*LES* is in better agreement with measurements than *RANS* and *URANS*
Kang and van Hooff (2022) [33]	Non-isothermal side-wall jet	*RANS/Standard k-ε*, *Realizable k-ε*, *RNG k-ε*, *LRN k-ε*, *RSM (SW)*, *RSM (BSL)*, and *SST k-ω*	Comparison of measured with three-hot-wire anemometer and predicted dimensionless velocity magnitude, air temperature, and turbulence kinetic energy	*SST k-ω* is the optimal turbulence model for CFD calculations in a room with a non-isothermal supplied jet
Thysen et al. (2021) [34]	Two opposing plane wall jets in an empty airplane cabin	*RANS/RNG k-ε*, *LRN k-ε*, *SST k-ω* *LES/WALE*, and *kinetic energy subgrid scale*	Comparison of measured with PIV [3] and predicted contour maps, mean decay of dimensionless maximum velocity, and jet growth profiles	*RANS* is in acceptable agreement with measurements; *SST k-ω* performs better than the *k-ε*; *LES* performed much better than *RANS*
Sánchez et al. (2020) [35]	Ventilated façade	*Sparlat–Allmaras*, *Standard k-ε*, *RNG k-ε*, *REA k-ε*, *Standard k-ω*, *SST k-ω*	Comparison of measured with PIV [3] vertical velocity component profiles	*RNG k-ε* model is in the best agreement with measurements
Morozowa et al. (2020) [36]	Differentially heated cavity, mixed convection	Direct numerical simulation (*DNS*) *No-model* *LES/WALE* and *S3PQ* *URANS/Standard k-ε* and *SST-k-ω*	Comparison of calculated global, integral airflow quantities: Nusselt number, stratification, kinetic energy, enstrophy, and average temperature, with reference values obtained in *DNS* simulation	*LES* and no-model predict global, integral airflow quantities with higher accuracy than *URANS*
Khayrullina et al. (2019) [37]	Impinging plane jets	*RANS/Standard k-ε*, *Realizable k-ε*, *RNG k-ε*, *SST k-ω* and *Reynolds stress* model	Comparison of velocity distributions predicted and measured using PIV [3]	The differences in the validation metric are negligibly small. It is impossible to distinguish the best model
Lestinen et al. (2019) [38]	Two plane opposed jets	*URANS/SST k-ω*, *hybrid RANS-LES*—detached eddy simulation (*DES*), hybrid *RANS-LES* stress-blended eddy simulation (*SBES*)/*SST-k-ω RANS* was merged with *LES*	Comparison of velocity distributions predicted and measured using LVTA [2]	There are no final conclusions regarding the preferred turbulence model

Table 2. *Cont.*

Authors (Year) [Ref.]	Type of Airflow in Room	Method/Turbulence Model	Validation Method	Conclusion/Preferred Method and Turbulence Model
Kosutova et al. (2018) [39]	Non-isothermal mixing ventilation in an enclosure with a heated floor	*RANS/RNG k-ε*, *Low Reynolds number k-ε*, *SST k-ω*, *Std k-ω* and *RSM*	Comparison of velocity distributions predicted and measured using LDA [1] and temperature distributions predicted and measured using thermocouples	*Low-Reynolds-number k-ε* performed best in velocity prediction. Temperature was most accurately reproduced by *SST k-ω*
Kobayashi et al. (2017) [40]	Impinging jet	*RANS/Standard k-ε*, *RNG k-ε*, *SST k-ω*, and *Low-Re SST k-ω*	Comparison of measured and predicted vertical profiles of velocity, turbulent kinetic energy, and temperature; velocity measured with hot wire and ultrasonic anemometers	*SST k-ω* is optimal for accuracy and computational economy
Moureh and Yataghene (2017) [41]	Air curtain	*RANS/Standard k-ε*, *LES/Dynamic Smagorinsky subgrid scale*	Comparison of velocity distributions predicted and measured using LDA [1] and PIV [3]	*LES* predicts jet characteristics better than *RANS k-ε*, but *LES* strongly underestimates the jet deviation outwards in comparison with PIV [3]
van Hooff et al. (2017) [42]	Cross ventilation	*RANS/Standard k-ε*, *RNG k-ε*, *Realizable k-ε*, *SST k-ω*, *RSM* *LES/Dynamic Smagorinsky subgrid scale*	Comparison of measured with constant temperature anemometry system and predicted parameters: mean velocity, turbulent kinetic energy, ventilation flow rate, and spreading width	*RANS* models fail to reproduce turbulent kinetic energy, *LES* better reproduces velocity, turbulence kinetic energy and volume flow rate
Achari and Das (2015) [43]	Impinging plane jet	*RANS/Standard k-ε*, *Low Reynolds number k-ε* proposed by Launder and Sharma (*LS*) and Yang and Shih (*YS*), *standard k-ω*	Comparison of calculated velocity component profiles with literature experimental data	*Low-Reynolds-number k-ε* Yang and Shih (*YS*) performed best
Hurnik et al. (2015) [44]	Sidewall jet, recirculating flow in the occupied zone	*RANS/Standard k-ε with enhanced wall treatment*	Comparison of predicted local, gross, and integral parameters in the jet and occupancy zones with LDA and LVTA measurements	Reproduction of the jet momentum is necessary for accurate air speed modeling in the occupied zone
Miltner et al. (2015) [45]	Straight and slightly rotating turbulent free jets	*RANS/One-equation*, *Standard k-ε*, *RNG k-ε*, *Realizable k-ε*, *Standard k-ω*, *SST* and *RSM*	Comparison of velocity distributions predicted and measured using LDA	The best results of validation in terms of axial and tangential velocity components and turbulence intensity are obtained with *RSM*

[1] LDA—laser Doppler anemometer. [2] LVTA—low-velocity thermal anemometer. [3] PIV—particle image velocimetry.

In the studies presented in Table 2 and within several older papers, the air movement in the room was caused by air jets such as plane jets [41,46], plane wall jets [31,34,36,38,39,46], 3D circular quasi-free sidewall jets [32,33,42,44], impinging jets [37,40,43], slightly swirling free jets [45], and confluent jets [47]. In order to validate the CFD results in the jet zone, the air velocity measurements were performed using LDA [32,40,41,44,45], a hot-wire anemometer [40,42], a three-hot-wire anemometer [33], PIV anemometry [34,37,41], a low-velocity thermal anemometer (LVTA) [38], and an ultrasonic anemometer [40]. In a previous paper [31], *RANS* CFD results were validated using *LES* results. Direct numerical simulation (*DNS*) results were used as reference data for *URANS* and *LES* validation [36]. Most of the studies presented in Table 2 analyzed the usefulness of *RANS* turbulence models; three cases concerned *URANS* models and half of the cases involved *LES* models.

1.3. Methods of CFD Validation

Most of the papers listed in Table 2 include, among other things, a comparison of calculated and measured flow parameters in the form of contour maps and profiles. This comparison is rather qualitative and its usefulness in selecting a turbulence model when providing more accurate results is questionable.

Previous papers [33,37,39,42] presented a quantitative comparison based on determining the validation metrics *FAC*(H). These metrics describe the fraction of the data within the range $(1/H; H)$:

$$FAC(H) = \frac{1}{n}\sum_{i=1}^{n} B \; for \; B = \begin{Bmatrix} 1 \; for \; 1/H \leq \frac{predicted\ value_i}{measured\ value_i} \leq H \\ 0 \; else \end{Bmatrix} \tag{10}$$

where H = 1.05, 1.1, 1.25, 1.3, 1.5, or 2.

In some cases, the global and integral parameters were used to quantitatively compare the CFD results. In an earlier paper [36], predicted values of the Nusselt number, stratification, average temperature, and average kinetic energy were quantitatively compared with the reference data.

In other previous work [32,44], the maximum mean velocity $\overline{U}_{xm}$, jet width R, and momentum flux M were used to validate the CFD predictions. These gross and integral parameters, that characterize the velocity distribution in the jet at a certain distance from the inlet, are presented in more detail in Section 2.3.

Average Speed in Occupied Zone Versus Jet Momentum Flux

So far, the benchmark test [48] has been used to validate CFD results for three types of turbulence models, i.e., *RANS Std k-ε* model [44], unsteady Reynolds-averaged Navier–Stokes (*URANS*), and vortex-resolving large eddy simulation *LES* [32]. The *RANS Std k-ε* model was used for two cases (denoted A and B) with different boundary conditions. The *LES* results with 16 and 35 million cells were analyzed. In the case of the benchmark test [48], the jet can be considered quasi-free at a distance x/D_e = 10–32 and, in this region, the airflow can be approximated using a point source of momentum model (PSM). Based on the available data, the relationship between the average air speed in the occupied zone, $\overline{W}_{aver}$, and the square root of the jet momentum flux $(M/\rho)^{1/2}$ is determined, see Figure 1.

Figure 1 confirms that the average air speed in the occupied zone, $\overline{W}_{aver}$, is very highly correlated with the square root of the jet momentum flux $(M/\rho)^{1/2}$. Incorrect modeling of the momentum flux may result in the classification of a room's thermal conditions into the wrong category. To avoid this, the modeling uncertainty of the square root of momentum flux $(M/\rho)^{1/2}$ should be less than about 5%.

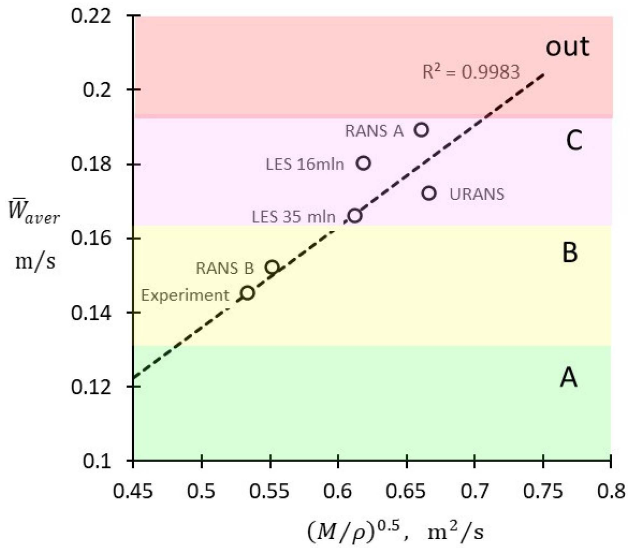

Figure 1. Correlation between the average mean speed in the occupied zone and the square root of momentum flux of the jet. Source of data: Experiment, *URANS*, *LES* 16 and 35 million [32], *RANS* A and B [44]; color scale: category of thermal local discomfort due to draft *DR*; category A—*DR* < 15%; category B—*DR* < 20%; category C—*DR* < 25%; assumed air temperature—20 °C; and turbulence intensity 40%.

1.4. Recommended Turbulence Models

In all cases comparing the *RANS* and *URANS* models with the results of the *LES* approach it was found that the *LES* results better reproduce the tested airflows in the room. In previous work [33,34,39,40], it was indicated that the *RANS/SST k-ω* model better agreed with measurement data compared to other *RANS* models. Earlier studies [37,38] did not identify the best turbulence model among the *RANS* models. Recent studies were mainly based on a statistical approach when estimating the uncertainties arising from the adopted turbulence model, whereas data-driven methods were predominantly used to reduce these uncertainties. In a prior paper [31], a data-driven *RANS* nonlinear model with coefficients of high-order terms determined using an artificial neural network was proposed. Three indoor airflows were selected as a training set, and four other flows were used to verify the model. The results show that this model can better predict anisotropic indoor flows.

Based on a review of the literature, it can be stated that *LES* modeling undeniably provides more accurate and reliable results than *RANS*. However, the *LES* models require higher computational costs and are more time consuming. Therefore, the LES method is rarely used in engineering applications. The author of ref. [49] concluded that *RANS* models are not obsolete because *RANS* is still widely used in engineering research and practice. Although *LES* is superior in its own right, it incurs greater simulation complexity and significantly higher computational costs. In the review conducted in ref. [12], the authors stated that CFD simulations of industrial flows in the coming decades will still mostly be based on the *RANS* turbulence model, and the uncertainties in the *RANS* model will remain a major obstacle to the predictive ability of these simulations. Thus, quantifying uncertainties in *RANS* predictions is essential to achieving the goal of certified CFD simulations.

In the case of the benchmark test [48], the jet can be considered quasi-free at a distance of x/D_e = 10–32. In this region, the airflow in the jet can be approximated and compared using a point source of momentum model (PSM). So far, this benchmark test has been used to validate CFD results for three types of turbulence models, i.e., the *Std k-ε* model available in the Fluent Airpak 3.0.16 commercial code [44], unsteady Reynolds-averaged Navier–Stokes (*URANS*) [32], and vortex-resolving large eddy simulation (*LES*) [32]. The last two are available in ANSYS Fluent.

The aim of the tests presented here is the qualitative and quantitative assessment of the results of the CFD calculation of airflow in a sidewall jet based on benchmark data [48]. The tests were carried out with steady-state conditions using seven Eddy–Viscosity Models (*EVM*) available in the ANSYS CFX 22.1 software. The goal was to find an *EVM* turbulence model that could provide the most similar results to the experiment and CFD results obtained with the *LES* turbulence model. So far, no validation of the CFD calculations for such cases has been performed.

2. Methods

2.1. Benchmark of a Room with a Sidewall Jet

The geometry of the test room with a sidewall jet, which was proposed by Hurnik et al. [48] for CFD validation, is shown in Figure 2. The room's dimensions correspond to a medium-sized office or living room. The air was supplied from a rectangular opening with the dimensions 0.144 m × 0.096 m and the velocity U_o = 5.16 m/s. The measurements were performed both in the jet region and in the occupied zone. A two-dimensional laser Doppler anemometer was used to measure velocity components in the jet region in two perpendicular planes (Figure 2). In the occupied zone, the air velocity was measured using a low-velocity thermal anemometer with omnidirectional sensors. A detailed description of the benchmark and the full set of measurement results are presented in earlier papers [44,48].

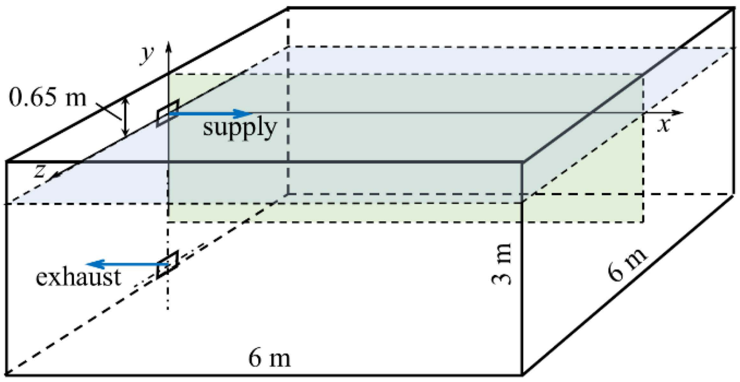

Figure 2. Tested room and the measurement planes in the jet zone.

2.2. Numerical Method

Numerical calculations were carried out with the use of Ansys CFX 22.1 software in steady-state and isothermal conditions for half of the test room due to its symmetry (Figure 2). The dimensions of the modeled half of the air supply opening were 0.072 m × 0.096 m (1/2 width × height). The intensity of the turbulence in the opening was set equal to 5%. The Navier–Stokes differential equations were discretized using the Finite Volume Method. The second-order upwind discretization scheme and Rhie–Chow algorithm were employed to couple pressure and velocity. Wall functions with the no-slip boundary condition were adopted. The Auto Timescale control option was selected with the conservative Length Scale and the Timescale Factor set to a default value of 1. Boundary conditions for the conducted numerical simulations are presented in Table 3.

The grid independence test was carried out with the use of the standard *k*-ε model. Three variants of discretization grids consisting of tetrahedral elements were tested. Their parameters are listed in Table 4. In each of the variants a boundary layer with a maximum thickness of 0.6 m was used in which the mesh size was equal to 0.01 m. In addition, mesh refinement was implemented on the surface of the inlet with a mesh edge length of 0.01 m. In the G1 variant, a default discretization grid with a mesh edge length of 0.3 m was used. In the G2 variant, the length of mesh edge was reduced to 0.1 m. In the G3 variant, additional mesh refinement was implemented in the supply jet axis with a refinement radius of 0.6 m and the length of the refined mesh edge being 0.01 m.

Table 3. Boundary conditions.

Boundary Condition	Value/Description
Analysis type	Steady state
Supply air speed	5.16 m/s
Inlet turbulence intensity	5%
Heat transfer	Isothermal
Air temperature	23 °C
Outlet relative pressure	1 Pa
Outlet pressure profile blend	0.05
Outlet pressure averaging	Average over whole outlet
Boundary condition	No slip wall
Wall roughness	Smooth wall
Reference domain pressure	101,325 Pa

Table 4. Tested discretization grid variants.

Discretization Grid Variant	Mesh Edge Length	Refinement Mesh Edge Length	Number of Elements
G1	0.3 m	-	4.10×10^4
G2	0.1 m	-	4.95×10^5
G3	0.1 m	0.01 m (refinement radius 0.6 m)	3.51×10^7

Numerical calculations carried out with the use of all discretization grid variants were validated with the use of experimental results [48] in the jet region (Figure 3). The best concurrence of the results was obtained with the use of G3 variant grid. The distribution of the mean axial velocity component $\overline{U}_x$ was the most similar to the measured one, both in terms of its maximum value and its profile. The results obtained with the use of the G2 grid variant were similar to the G3 variant, but the range of maximum values was higher and the air velocity profile was wider in the G2 variant. The G1 grid variant was not able to accurately reproduce the air velocity profile, which could have been affected by the large mesh size. Therefore, the G3 grid variant was adopted in the research on turbulence models.

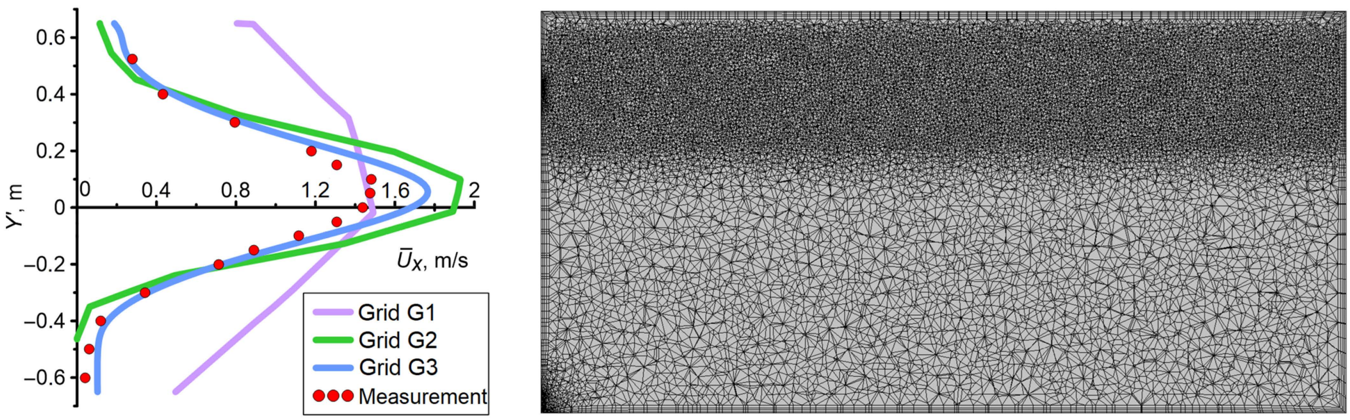

(**a**) (**b**)

Figure 3. Comparison of the measurement data with the CFD results obtained with the use of three discretization grid variants for the standard k-ε turbulence model in a jet region; distribution of the mean axial velocity component $\overline{U}_x$ for x/D_e = 20.8 (**a**) and the G3 discretization grid; cross-section in a plane passing through the center of the inlet (**b**).

In order to evaluate the numerical model's quality, a convergence assessment of the numerical solution was conducted. The residual is the most important determinant of numerical solution convergence as it directly reflects the accuracy of an equation's solution [50]. The root mean square residuals of pressure and velocity were selected to assess when convergence was reached. The value at which the pressure and velocity root mean square residuals stabilized for all the *k-ω* models was 1×10^{-7}, for the *k-ε* models it was 8×10^{-8} (i.e., the standard *k-ε* model) and 4×10^{-7} (i.e., the *RNG k-ε* model), and, for the one-equation *EVTM* model it was 1×10^{-7}. According to [50], root mean square residual levels of value 1×10^{-6} or lower show a very tight convergence and are sufficient for engineering applications.

The number of iterations after which the monitored parameters in the jet and the boundary layer region stabilized (velocity components, turbulent kinetic energy, and turbulent dissipation rate—except for models where turbulent kinetic energy is absent) was in the range of 1.2×10^3 for the *EVTM* model to 1×10^4 for the *SST* model. The relative wall distance value $y+$ was lower than 15 for all turbulence models analyzed.

2.3. Local, Gross, and Integral Parameters

The CFD results are most often validated by comparing profiles of local velocity parameters such as mean velocity $\overline{U}$, mean velocity components $\overline{U}_x$, $\overline{U}_y$, $\overline{U}_z$, and standard deviations of velocity fluctuations u_x^*, u_y^*, u_z^* in selected jet cross-sections. This method of validation can also be called point-to-point comparison. More reliable and representative validation can be carried out by comparing gross and integral jet parameters. Gross parameters, i.e., maximum mean velocity $\overline{U}_{xm}$, position of the maximum mean velocity y_m, and jet width R, and integral parameters, i.e., volume flux V and momentum flux M, characterize the airflow in the jet at a certain distance from the supply opening.

In the benchmark tests, the jet is supplied from the rectangular opening and affected by the ceiling; therefore, it cannot be treated as an axisymmetric jet. Due to the Coanda effect, the position of the point of maximum velocity y_m changes with the distance from the opening and has to be identified. The values of the mean axial air velocity component $\overline{U}_{xm}$, measured and calculated in several cross-sections of the turbulent jet region, were approximated using a quasi-Gaussian exponential curve:

$$\overline{U}_x = \overline{U}_{xm} \cdot exp\left[-(r/R_\alpha)^{7/4}\right] \tag{11}$$

The radial distance from the jet axis position equals:

$$r = \left[(z - z_m)^2 + (y - y_m)^2\right]^{1/2} \tag{12}$$

To describe the velocity distribution in an asymmetric air jet, the angular change in the velocity profile width should be considered. In the case of the CFD results, it was possible to analyze the radial changes in the velocity in the 180° range covered by the CFD data and 180° covered by the assumption of the flow symmetry in the z-plane. In this case, the jet profile width was calculated as a trigonometric series of six harmonic components:

$$R_\alpha = R(1 + a_1\, cos\alpha + a_2\, cos2\alpha + a_3\, cos3\alpha + a_4\, cos4\alpha + \cdots) \tag{13}$$

The angle α is found in this expression, the explicit form of which is given by:

$$\alpha = arctan2[(z - z_m), (y - y_m)]. \tag{14}$$

The set of parameters $\overline{U}_{xm}, R,\ y_m,\ z_m, a_1, \ldots a_6$, describing the distribution of the mean axial velocity component at different distances from the inlet opening x, were found by a least-squares method using the SOLVER procedure in EXCEL. Next, the air velocity in the quasi-free jet zone was approximated by the model of the jet from a point source of momentum. The set of equations for the PSM model with the profile exponent $n = 1.75$ is presented in Table 5. The gross parameters are jet spread coefficient α, position of the jet origin x_o/D_e, and coefficient of momentum loss K_M, which characterize the whole jet in the quasi-free region.

Table 5. Model of a free axisymmetric jet generated by a point source of momentum (PSM) model.

Definition	Equation	#
Jet spread	$R = a(x - x_o)$	(15)
$\overline{U}_x$ velocity profile	$\overline{U}_x/\overline{U}_{xm} = exp\left[-(r/R)^{7/4}\right]$	(16)
M/ρ in PSM (constant)	$M/\rho = 1.5210\ \overline{U}_{xm}^2 R^2$	(17)
Boundary momentum flux	$M_o/\rho = A_o\ U_o^2 = (\pi\ D_e^2/4)U_o^2$	(18)
Conservation of momentum flux	$(M/M_o)^{1/2} = K_M$	(19)
Decay of $\overline{U}_{xm}$	$\overline{U}_{xm}/U_o\ = K_M\ [0.7186\ /a]/[(x - x_o)/D_e]$	(20)

3. Results

3.1. Maps and Profiles of Mean Axial Velocity Component

Figure 4 shows contour maps of the mean axial air velocity component $\overline{U}_x$'s distribution in the supply air jet normalized by the inlet velocity U_o = 5.16 m/s. The maps were prepared using measurement data and the CFD calculation results with the use of *EVM* turbulence models. The area on the maps limited by 1% isoline is the background of the jet. The map for the zero-equation model significantly differs from the maps for the other *EVM* turbulence models and is characterized by a much shorter range for all of the isolines. Therefore, the results for the zero-equation model were excluded from further analyses.

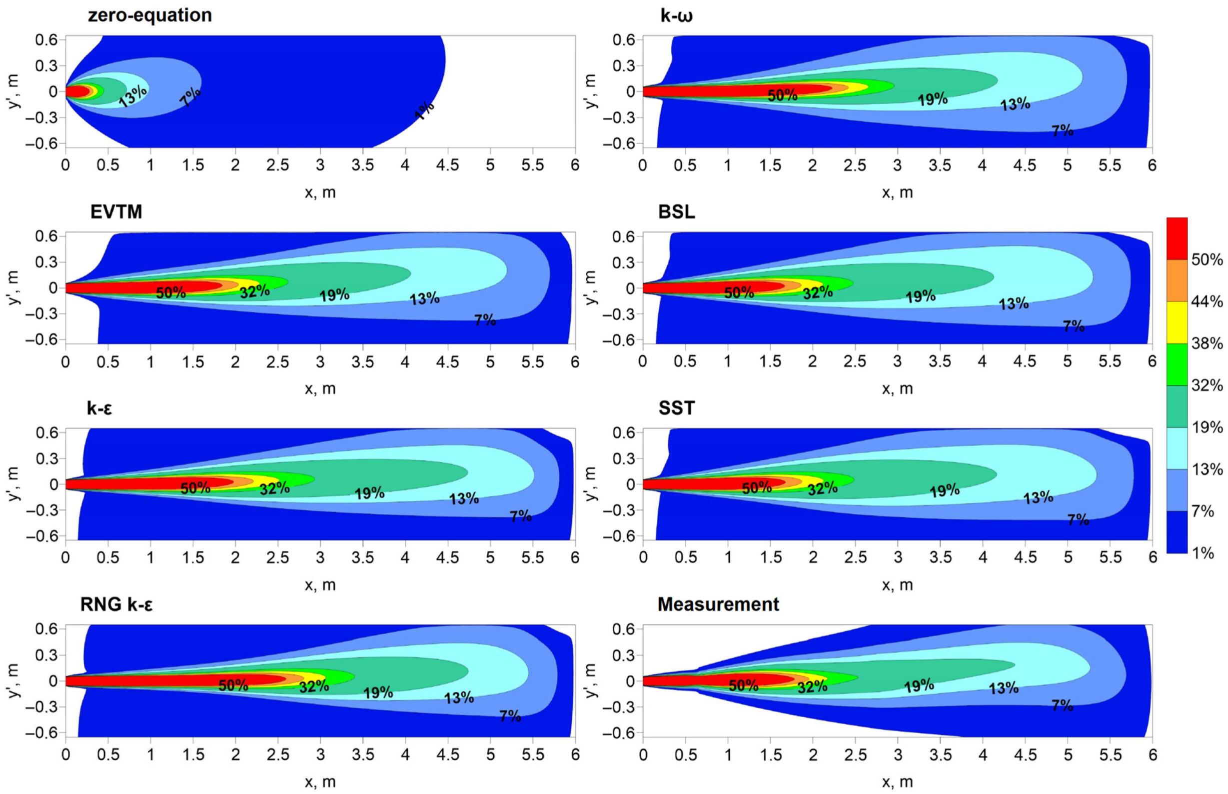

Figure 4. Contour maps of the normalized axial mean air velocity component $\overline{U}_x/U_o$ in the plane cross-section z = 0 for the *EVM* turbulence models and measurement data.

The vertical jet profiles of the axial mean air velocity component are deformed due to the deflection of the air jet towards the ceiling. Therefore, the profiles in the horizontal plane y = 0 at a distance from the inlet equal to x = 2.79 m (x/D_e = 20.8) were selected for comparison, see Figure 5. The results of measurements and CFD calculations were approximated by an exponential curve in a form corresponding to:

$$\overline{U}_x = \overline{U}_{xm}\ |_{x=2.79;\ y=0} \cdot e^{-(|z|/R|_{x=2.79;\ y=0})^{7/4}} \tag{21}$$

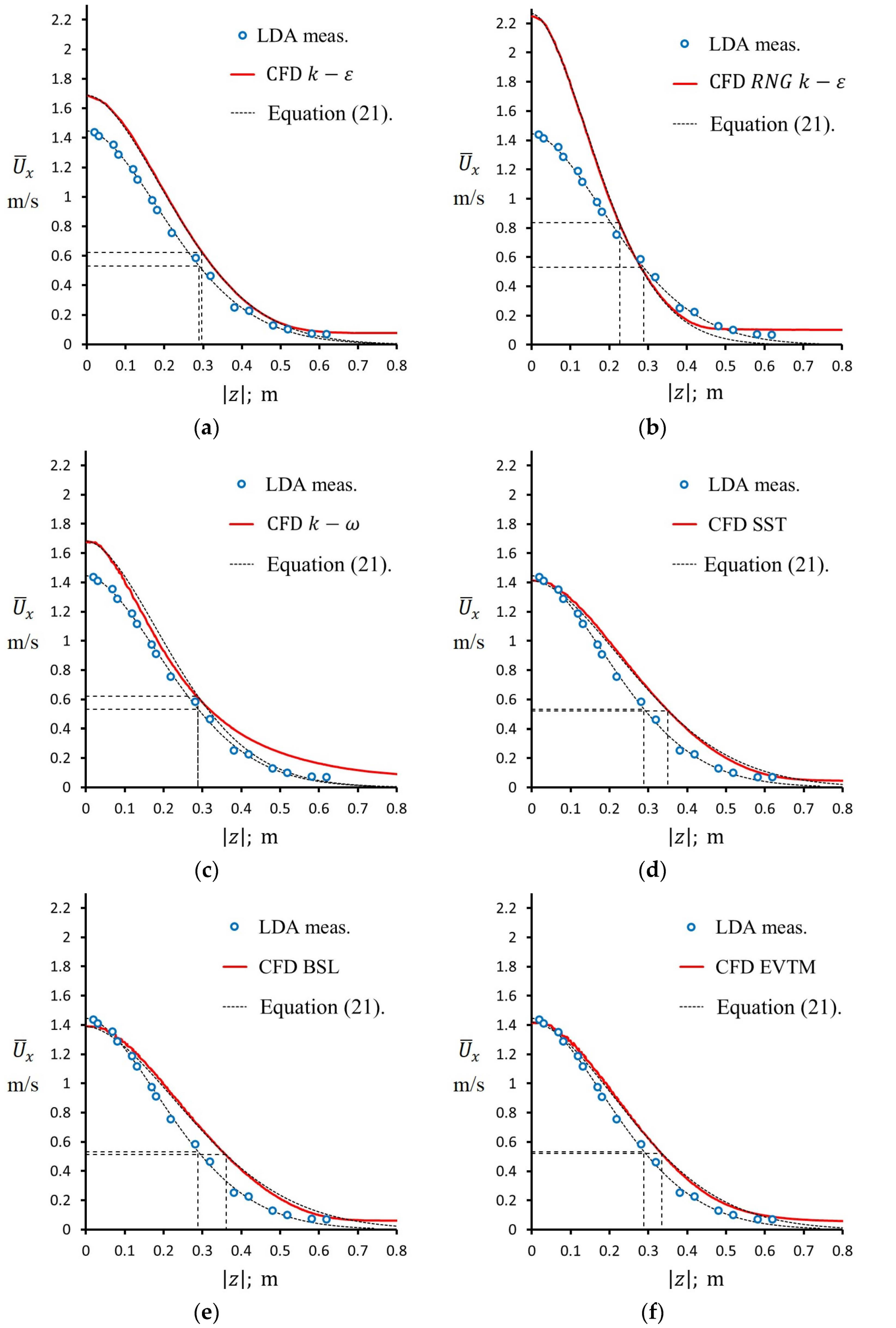

Figure 5. Axial mean air velocity component profiles in the horizontal plane with $y = 0$ and $x = 2.79$ m (i.e., $x/D_e = 20.8$). Turbulence models: (**a**) *k-ε*; (**b**) *RNG k-ε*; (**c**) *k-ω*; (**d**) *SST*; (**e**) *BSL*; (**f**) *EVTM*.

Two parameters were obtained as a result of the approximation for the compared profiles, i.e., the maximum value of the axial velocity component $\overline{U}_{xm}\,|_{|x=2.79;\ y=0}$ and the jet profile width $R|_{|x=2.79;\ y=0}$. Thus, it was possible to compare the analyzed profiles quantitatively. The approximation lines are marked in Figure 5 with dashed black lines.

3.2. Gross and Integral Parameters in the Quasi-Free Jet Zone

The distributions of the gross and integral parameters of the air jet for a certain distance from the inlet are shown in Figure 6. The parameters of the point source of momentum (PSM) model obtained by an approximation of the air velocity distribution in the quasi-free zone of the jet are presented in Table 6.

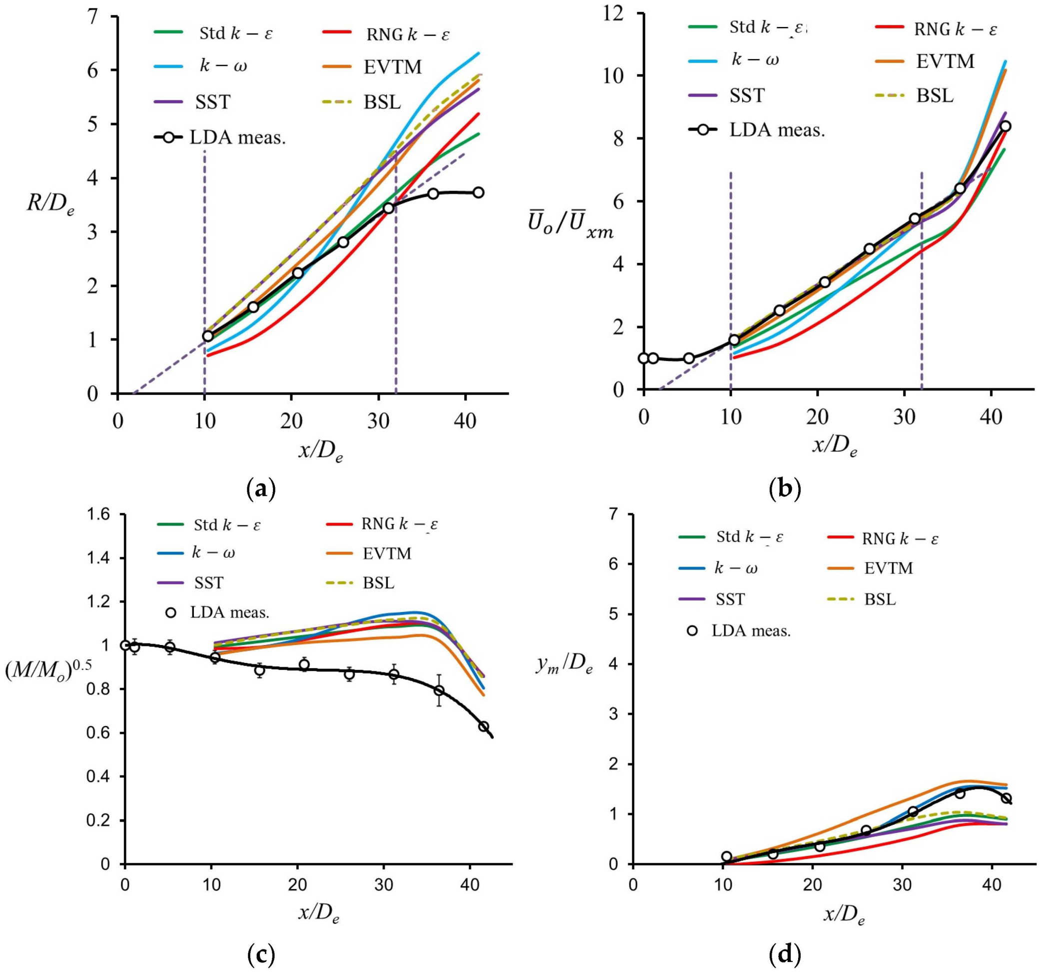

Figure 6. Changes in the gross and integral parameters of the jet for the distance from the inlet: (**a**) the jet width R/D_e; (**b**) the ratio of inlet velocity and maximum mean axial velocity $U_o/\overline{U}_{xm}$; (**c**) the square root of jet momentum flux $(M/M_o)^{1/2}$; and (**d**) the vertical position of the maximum mean velocity y_m/D_e.

Table 6. Parameters of the point source of momentum (PSM) model obtained by an approximation of the air velocity distribution in the quasi-free zone of the jet.

	x_o/D_e	a	K_M
LDA	1.8	0.117	88.4%
LES [32]	2.2	0.130	100.6%
k-ω	4.6	0.138	103.4%
Std k-ε	2.0	0.118	104.0%
RNG k-ε	4.0	0.105	102.9%
EVTM	3.0	0.137	100.6%
BSL	1.9	0.143	106.4%
SST	2.5	0.148	106.5%

A comparison of the *EVM* and *LES* results in the quasi-free jet region with the outcomes of the measurements using LDA is presented in Table 7. The quantities $\Delta(x_o/D_e)$, $\delta(a_u)$, and $\delta(K_M)$ represent the absolute differences in the position of the jet origin, relative differences in the jet spread coefficient, and relative differences in the momentum losses coefficient, i.e.,

$$\Delta(x_o/D_e) = (x_o/D_e)\,|^{\,\mathrm{EVM}} - (x_o/D_e)\,|^{\,\mathrm{LDA}}, \quad (22)$$

$$\delta(a_u) = (a\,|^{\,\mathrm{EVM}} - a\,|^{\,\mathrm{LDA}})/a\,|^{\,\mathrm{LDA}}, \quad (23)$$

$$\delta(K_M) = (K_M\,|^{\,\mathrm{EVM}} - K_M\,|^{\,\mathrm{LDA}})/K_M\,|^{\,\mathrm{LDA}}. \quad (24)$$

Table 7. Comparison of the *EVM* results in the quasi-free jet region with the outcomes of the measurement using the LDA.

Turbulence Model	Linear Jet Spread	Inverse Changes of Maximum Velocity	"Gaussian" Radial Profile of Velocity	$\Delta(x_o/D_e)$	$\delta(a)$	$\delta(K_M)$
LDA	+	+	+	0.0	0.0%	0.0%
LES [25]	+	+	+	0.4	11.1%	13.8%
k-ω	–	–	–	2.8	17.9%	17.0%
Std k-ε	+	+	+	0.2	0.9%	17.6%
RNG k-ε	–	–	–	2.2	−10.3%	16.4%
EVTM	+	+	+	1.2	17.1%	13.8%
BSL	+	+	+	0.1	22.2%	20.4%
SST	+	+	+	0.7	26.5%	20.5%

4. Discussion

The results of the LDA measurements confirmed that the tested jet at a distance x from 1.3 m to 4.2 m (x/D_e from 10 to 32) behaves like a quasi-free jet, which is proved by:

- The self-similarity of the mean velocity distribution, as given in Equation (11);
- The linear spread of the jet, as provided in Equation (15);
- The fact that they are inversely proportional to distance velocity decay, as given in Equation (20).

The maps for all the *EVM* turbulence models, see Figure 4, provided a qualitatively similar but not identical picture of the velocity field in the jet zone. Based on these maps, it is not possible to accurately determine the throw length of the jet because the isolines for less than 0.5 m/s terminate in the jet impingement zone, i.e., less than 1.8 m from the opposite wall. Comparing the contour maps $\overline{U}_x/U_o$ for the *BSL* and *SST* models, it is noteworthy that they are very similar. Examining the maps, it can also be seen that all the maps show a slight deflection of the jet towards the ceiling. Determining the other global parameters, such as x_o, R, and $\overline{U}_{xm}$, based on these maps, it is clear that they may include significant errors. Therefore, it can be concluded that the maps have little usefulness in the validation of the CFD results.

The profiles of the axial mean air velocity component in the middle of the quasi-free jet zone, when the horizontal plane y = 0 and the distance x = 2.79 m (i.e., $x/D_e = 21$), are presented in Figure 5. As shown in Figure 4, the maximum mean axial velocity $\overline{U}_{xm}\,|_{x=2.79;\ y=0}$ valued obtained for the *EVTM*, *BSL*, and *SST* models were very close to the measured one but, at this distance, the jet profile widths $R|_{x=2.79;\ y=0}$ were greater than the measured one by 10%, 24%, and 21%, respectively. The measured jet profile width $R|_{x=2.79;\ y=0}$ and the one calculated with the use of the *k-ω* and *Std k-ε* models differed very little, but the maximum mean axial velocity $\overline{U}_{xm}\,|_{x=2.79;\ y=0}$ was higher than the measured one by 20%. The results obtained for the *RNG k-ε* model varied the most from the measurements, both in terms of $\overline{U}_{xm}\,|_{x=2.79;\ y=0}$ and $R|_{x=2.79;\ y=0}$. The quantitative comparison of the velocity profiles presented in Figure 5 did not provide unambiguous and conclusive arguments that allowed for the assessment of the usefulness of the analyzed turbulence models. Therefore, an in-depth comparative analysis of the gross and integral parameters, as well as parameters for the free jet model generated by the point source of momentum (PSM), was needed. The results of this analysis are presented in Figure 6 and Tables 6 and 7.

In the quasi-free jet zone, the jet width increases linearly and the maximum velocity decreases inversely with the distance from the jet origin. Therefore, as seen in Figure 6a,b, the R/D_e and $U_o/\overline{U}_{xm}$ values changed linearly. Such a linear relationship can be observed for the *EVTM*, *Std k-ε*, *BSL*, and *SST* turbulence models but not for the *k-ω* and *RNG k-ε* models. The best agreement between the measurement and calculations was obtained for the *EVTM* and *Std k-ε* turbulence models. However, while the *EVTM* model accurately reproduced $\overline{U}_{xm}$, it overestimated R by 17%. The *Std k-ε* model performed in an opposite way, i.e., it overestimated $\overline{U}_{xm}$ by 17% and precisely predicted R. The changes in the momentum flux $(M/M_o)^{1/2}$ are shown in Figure 6c. All the turbulence models overestimated the measured value of this flux. The least overestimated results were obtained for the *EVTM* model. Figure 6d shows the changes in the vertical position of the maximum mean velocity y_m/D_e. All the turbulence models reproduced the deflection of the air jet towards the ceiling with satisfactory accuracy.

The highest discrepancies in the calculated and measured positions of the jet's origin x_o/D_e were obtained with the *k-ω* and *RNG k-ε* models, and the best compliance was obtained with the *Std k-ε* and *BSL* models. The coefficient a_u that characterized the jet spread was modeled with the best accuracy using the *Std k-ε* turbulence model.

In order to correctly model the air distribution in the occupied zone of the room, it is necessary to accurately reproduce the momentum flux of the supply air jet. The velocity in the occupied zone is directly proportional to the square root of the momentum flux $(M/\rho)^{1/2}$ [4]. Thus, the momentum loss coefficient K_M determined by the CFD calculations should be as close as possible to the measured one. Considering this criterion, optimal compliance was obtained for the *EVTM* turbulence model. In this case, the K_M coefficient and, consequently, the air velocity in the occupied zone were about 12% higher than the measured values.

The analysis presented in Table 7 shows that the *k-ω* and *RNG k-ε* turbulence models did not correctly reproduce the jet spread, the decay of the maximum velocity, and the velocity profile in the jet cross section and, therefore, cannot be recommended to simulate velocity distribution in a quasi-free jet region. The *BSL* and *SST* models calculated air distribution parameters with errors higher than 20%. The results obtained with the standard *Std k-ε* and *EVTM* models were most similar to the measurement data since their errors slightly exceeded 15%. Comparing the results of the CFD calculations using the *EVM* turbulence models with those of the *LES* calculations, a good agreement between the *EVTM* and *LES* results can be observed.

5. Conclusions

In the presented studies, numerical CFD modeling of an air jet supplying air from the sidewall to the room was carried out using seven *EVM RANS* turbulence models. Validation of CFD results was performed based on experimental data [48]. This case represents a typical office or residential room. A comparative analysis of gross and integral parameters, as well as parameters of the quasi-free jet model generated by a point source of momentum, was carried out. Based on the obtained results, the following conclusions can be drawn.

Jet spread, the decay of the maximum velocity, and the velocity profile in the jet cross-section were not correctly reproduced by the *k-ω* and *RNG k-ε* models. Therefore, they cannot be recommended for simulations of air velocity distribution in a quasi-free jet region.

The values of the global and integral parameters obtained with the standard *Std k-ε* and *EVTM* models were most similar to the experimental data. Their error values slightly exceeded 15%. These *EVM RANS* turbulence models can be effectively used in the HVAC industry to simulate air distribution in supplied air jets in the early conceptual stages of HVAC system design [36].

The greatest consistency in the momentum loss coefficient K_M was obtained for the *EVTM* turbulence model. Its value was overestimated by 12%, exactly the same value as in the case of the *LES* model.

The errors in the CFD simulations for the *BSL* and *SST* models were higher than 20%, which places these models in second place after the *Std k-ε* and *EVTM* models.

Further research on the use of the *EVM RANS* models could include a more thorough analysis of the air speed in the occupied zone to verify their applicability in the presence of people within a room.

Author Contributions: Conceptualization, M.H., P.C. and Z.P.; methodology, M.H. and Z.P.; software, P.C.; validation, M.H., P.C. and Z.P.; formal analysis, M.H. and Z.P.; data curation, P.C. and M.H.; writing—original draft preparation, M.H., P.C. and Z.P.; writing—review and editing, M.H., P.C. and Z.P.; supervision, Z.P. All authors have read and agreed to the published version of the manuscript.

Funding: This research received no external funding.

Data Availability Statement: Data are contained within the article.

Acknowledgments: The work was supported by the Polish Ministry of Education and Science within the research subsidy.

Conflicts of Interest: The authors declare no conflict of interest.

Nomenclature

a	jet spread coefficient (-)
B	boolean variable (-)
D	diameter (m)
H	upper limit value (-)
k	turbulence kinetic energy (m^2/s^2)
K	coefficient (-)
M	mean motion momentum flux in the axial direction ($kg{\cdot}m/s^2$)
n	number of samples (-)
r	radial distance from the jet axis (m)
R	radial width of the jet profile (m)
U	velocity (m/s)
W	speed (m/s)
x, y, z	Cartesian coordinates (m)
Greek symbols:	
ε	turbulence energy dissipation rate (m^2/s^3)
υ	viscosity coefficient (m^2/s)
ρ	density (kg/m^3)
ω	turbulence vorticity (1/s)
Subscripts:	
e	equivalent
i	axis of coordinate system, $i = x, y, z$
m	molecular, maximum
M	momentum
o	inlet, origin
t	turbulent

References

1. *ANSI/ASHRAE Standard 55*; Thermal Environmental Conditions for Human Occupancy. ANSI: Washington, DC, USA, 2023.
2. *ISO 7730:2005 (En)*; Ergonomics of the Thermal Environment—Analytical Determination and Interpretation of Thermal Comfort Using Calculation of the PMV and PPD Indices and Local Thermal Comfort Criteria. ISO: Geneva, Switzerland, 2005.
3. Hussein, T.; Löndahl, J.; Thuresson, S.; Alsved, M.; Al-Hunaiti, A.; Saksela, K.; Aqel, H.; Junninen, H.; Mahura, A.; Kulmala, M. Indoor Model Simulation for COVID-19 Transport and Exposure. *Int. J. Environ. Res. Public Health* **2021**, *18*, 2927. [CrossRef]
4. Cravero, C.; Marsano, D. Simulation of COVID-19 Indoor Emissions from Coughing and Breathing with Air Conditioning and Mask Protection Effects. *Indoor Built Environ.* **2022**, *31*, 1242–1261. [CrossRef]
5. Awbi, H.B. *Ventilation of Buildings*; Taylor & Francis: London, UK, 2003; ISBN 978-0-415-27056-4.

6. Jackman, P.J. *Air Movement in Rooms with Side-Wall Mounted Grilles: A Design Procedure*; Heating & Ventilation Research Association: London, UK, 1970.
7. *ANSI/ASHRAE Standard 113-2005*; Method of Testing for Room Air Diffusion. ANSI: Washington, DC, USA, 2005.
8. Yang, B.; Melikov, A.K.; Kabanshi, A.; Zhang, C.; Bauman, F.S.; Cao, G.; Awbi, H.; Wigö, H.; Niu, J.; Cheong, K.W.D.; et al. A Review of Advanced Air Distribution Methods—Theory, Practice, Limitations and Solutions. *Energy Build.* **2019**, *202*, 109359. [CrossRef]
9. Stern, F.; Wilson, R.V.; Coleman, H.W.; Paterson, E.G. *Verification and Validation of CFD Simulations*; Defense Technical Information Center: Fort Belvoir, VA, USA, 1999.
10. Chen, Q.; Srebric, J. A Procedure for Verification, Validation, and Reporting of Indoor Environment CFD Analyses. *HVAC&R Res.* **2002**, *8*, 201–216. [CrossRef]
11. Chen, Q. Editorial: Computer Simulations and Experimental Measurements of Air Distribution in Buildings: Past, Present, and Future. *HVAC&R Res.* **2007**, *13*, 849–851. [CrossRef]
12. Xiao, H.; Cinnella, P. Quantification of Model Uncertainty in RANS Simulations: A Review. *Prog. Aerosp. Sci.* **2019**, *108*, 1–31. [CrossRef]
13. Cravero, C.; De Domenico, D.; Marsano, D. Uncertainty Quantification Analysis of Exhaust Gas Plume in a Crosswind. *Energies* **2023**, *16*, 3549. [CrossRef]
14. Xia, L.; Zou, Z.-J.; Wang, Z.-H.; Zou, L.; Gao, H. Surrogate Model Based Uncertainty Quantification of CFD Simulations of the Viscous Flow around a Ship Advancing in Shallow Water. *Ocean Eng.* **2021**, *234*, 109206. [CrossRef]
15. Ansys CFX | Industry-Leading CFD Software. Available online: https://www.ansys.com/products/fluids/ansys-cfx (accessed on 24 April 2023).
16. Piomelli, U. Large Eddy Simulations in 2030 and beyond. *Phil. Trans. R. Soc. A* **2014**, *372*, 20130320. [CrossRef]
17. Zhai, Z.J.; Zhang, Z.; Zhang, W.; Chen, Q.Y. Evaluation of Various Turbulence Models in Predicting Airflow and Turbulence in Enclosed Environments by CFD: Part 1—Summary of Prevalent Turbulence Models. *HVAC&R Res.* **2007**, *13*, 853–870.
18. Zhang, Z.; Zhang, W.; Zhai, Z.J.; Chen, Q.Y. Evaluation of Various Turbulence Models in Predicting Airflow and Turbulence in Enclosed Environments by CFD: Part 2—Comparison with Experimental Data from Literature. *HVAC&R Res.* **2007**, *13*, 871–886.
19. Chen, Q.; Xu, W. A Zero-Equation Turbulence Model for Indoor Airflow Simulation. *Energy Build.* **1998**, *28*, 137–144. [CrossRef]
20. Wang, M.; Chen, Q. Assessment of Various Turbulence Models for Transitional Flows in an Enclosed Environment (RP-1271). *HVAC&R Res.* **2009**, *15*, 1099–1119.
21. Meslem, A.; Dia, A.; Beghein, C.; El Hassan, M.; Nastase, I.; Vialle, P.-J. A Comparison of Three Turbulence Models for the Prediction of Parallel Lobed Jets in Perforated Panel Optimization. *Build. Environ.* **2011**, *46*, 2203–2219. [CrossRef]
22. Hussain, S.; Oosthuizen, P.H.; Kalendar, A. Evaluation of Various Turbulence Models for the Prediction of the Airflow and Temperature Distributions in Atria. *Energy Build.* **2012**, *48*, 18–28. [CrossRef]
23. Stamou, A.; Katsiris, I. Verification of a CFD Model for Indoor Airflow and Heat Transfer. *Build. Environ.* **2006**, *41*, 1171–1181. [CrossRef]
24. Serra, N. Revisiting RANS Turbulence Modelling Used in Built-Environment CFD Simulations. *Build. Environ.* **2023**, *237*, 110333. [CrossRef]
25. Srebric, J.; Chen, Q. Simplified Numerical Models for Complex Air Supply Diffusers. *HVAC&R Res.* **2002**, *8*, 277–294. [CrossRef]
26. Cao, S.-J.; Meyers, J. Influence of Turbulent Boundary Conditions on RANS Simulations of Pollutant Dispersion in Mechanically Ventilated Enclosures with Transitional Slot Reynolds Number. *Build. Environ.* **2013**, *59*, 397–407. [CrossRef]
27. Tapsoba, M.; Moureh, J.; Flick, D. Airflow Patterns in a Slot-Ventilated Enclosure Partially Loaded with Empty Slotted Boxes. *Int. J. Heat Fluid Flow* **2007**, *28*, 963–977. [CrossRef]
28. Koskela, H.; Maula, H. A CFD Model of a Swirl Diffuser for Heating and Cooling Modes. *Int. J. Vent.* **2013**, *12*, 159–166. [CrossRef]
29. Susin, R.M.; Lindner, G.A.; Mariani, V.C.; Mendonça, K.C. Evaluating the Influence of the Width of Inlet Slot on the Prediction of Indoor Airflow: Comparison with Experimental Data. *Build. Environ.* **2009**, *44*, 971–986. [CrossRef]
30. Gurgul, S.; Fornalik-Wajs, E. On the Measure of the Heat Transfer Performance of RANS Turbulence Models in Single Round Jet Impingement. *Energies* **2023**, *16*, 7236. [CrossRef]
31. Chen, B.; Liu, S.; Liu, J.; Jiang, N.; Chen, Q. Application of Data-Driven RANS Model in Simulating Indoor Airflow. *Indoor Air* **2022**, *32*, e13123. [CrossRef] [PubMed]
32. Hurnik, M.; Ivanov, N.; Zasimova, M.; Popiolek, Z. Local and Gross Parameters of Air Distribution in a Room with a Sidewall Jet: CFD Validation Based on Benchmark Test. *Build. Environ.* **2022**, *207*, 108509. [CrossRef]
33. Kang, L.; van Hooff, T. Influence of Inlet Boundary Conditions on 3D Steady RANS Simulations of Non-Isothermal Mechanical Ventilation in a Generic Closure. *Int. J. Therm. Sci.* **2022**, *182*, 107792. [CrossRef]
34. Thysen, J.-H.; van Hooff, T.; Blocken, B.; van Heijst, G.J.F. CFD Simulations of Two Opposing Plane Wall Jets in a Generic Empty Airplane Cabin: Comparison of RANS and LES. *Build. Environ.* **2021**, *205*, 108174. [CrossRef]
35. Sánchez, M.N.; Giancola, E.; Blanco, E.; Soutullo, S.; Suárez, M.J. Experimental Validation of a Numerical Model of a Ventilated Façade with Horizontal and Vertical Open Joints. *Energies* **2020**, *13*, 146. [CrossRef]
36. Morozova, N.; Trias, F.X.; Capdevila, R.; Pérez-Segarra, C.D.; Oliva, A. On the Feasibility of Affordable High-Fidelity CFD Simulations for Indoor Environment Design and Control. *Build. Environ.* **2020**, *184*, 107144. [CrossRef]

37. Khayrullina, A.; van Hooff, T.; Blocken, B.; van Heijst, G. Validation of Steady RANS Modelling of Isothermal Plane Turbulent Impinging Jets at Moderate Reynolds Numbers. *Eur. J. Mech. B/Fluids* **2019**, *75*, 228–243. [CrossRef]
38. Lestinen, S.; Wesseling, M.; Kosonen, R.; Koskela, H.; Müller, D. Airflow Characteristics under Planar Opposed Ventilation Jets in a Controlled Indoor Environment. *E3S Web Conf.* **2019**, *111*, 01029. [CrossRef]
39. Kosutova, K.; van Hooff, T.; Blocken, B. CFD Simulation of Non-Isothermal Mixing Ventilation in a Generic Enclosure: Impact of Computational and Physical Parameters. *Int. J. Therm. Sci.* **2018**, *129*, 343–357. [CrossRef]
40. Kobayashi, T.; Sugita, K.; Umemiya, N.; Kishimoto, T.; Sandberg, M. Numerical Investigation and Accuracy Verification of Indoor Environment for an Impinging Jet Ventilated Room Using Computational Fluid Dynamics. *Build. Environ.* **2017**, *115*, 251–268. [CrossRef]
41. Moureh, J.; Yataghene, M. Large-Eddy Simulation of an Air Curtain Confining a Cavity and Subjected to an External Lateral Flow. *Comput. Fluids* **2017**, *152*, 134–156. [CrossRef]
42. van Hooff, T.; Blocken, B.; Tominaga, Y. On the Accuracy of CFD Simulations of Cross-Ventilation Flows for a Generic Isolated Building: Comparison of RANS, LES and Experiments. *Build. Environ.* **2017**, *114*, 148–165. [CrossRef]
43. Achari, A.M.; Das, M.K. Application of Various RANS Based Models towards Predicting Turbulent Slot Jet Impingement. *Int. J. Therm. Sci.* **2015**, *98*, 332–351. [CrossRef]
44. Hurnik, M.; Blaszczok, M.; Popiolek, Z. Air Distribution Measurement in a Room with a Sidewall Jet: A 3D Benchmark Test for CFD Validation. *Build. Environ.* **2015**, *93*, 319–330. [CrossRef]
45. Miltner, M.; Jordan, C.; Harasek, M. CFD Simulation of Straight and Slightly Swirling Turbulent Free Jets Using Different RANS-Turbulence Models. *Appl. Therm. Eng.* **2015**, *89*, 1117–1126. [CrossRef]
46. Heschl, C.; Inthavong, K.; Sanz, W.; Tu, J. Evaluation and Improvements of RANS Turbulence Models for Linear Diffuser Flows. *Comput. Fluids* **2013**, *71*, 272–282. [CrossRef]
47. Andersson, H.; Cehlin, M.; Moshfegh, B. A Numerical and Experimental Investigation of a Confluent Jets Ventilation Supply Device in a Conference Room. *Energies* **2022**, *15*, 1630. [CrossRef]
48. Hurnik, M.; Blaszczok, M.; Popiolek, Z. Air Speed and Velocity Measurements in a Room with a Sidewall Jet. *Data Brief* **2015**, *5*, 213–217. [CrossRef] [PubMed]
49. Blocken, B. LES over RANS in Building Simulation for Outdoor and Indoor Applications: A Foregone Conclusion? *Build. Simul.* **2018**, *11*, 821–870. [CrossRef]
50. *Ansys CFX-Solver Modeling Guide*; ANSYS, Inc.: Canonsburg, PA, USA, 2024.